CALIFORNIA POLYTECHNIC STATE UNIVERSITY (CAL POLY)

Technical Turbine Design Report

Aerodynamics Team
Josephine Maiorano (Lead)
Timothy Reyna
Mirada Huson

Electrical Team
Jonathan Yu (Lead)
Lily Goldman (Lead)
Nathan Jaggers
Aditi Lappathi
Zachariah Mustar
Kennedy Knoll
Charles Raney
Samantha Whalen

Team Lead – Zach Dunkelberger

Mechanical Team
Jeff Larson (Lead)
Trevor Ortega
Milo Klein
Max Scott
Alan Onuma
Ryan Singer
Elizabeth Costley
Nora Riedinger
James Cusanelli
Nico Nani
Andrew Walker

Advisors
Dr. Andrew Kean –
Principal Investigator
Prof. Dale Dolan –
Faculty Advisor
Dan Castro –
Senior Project Advisor

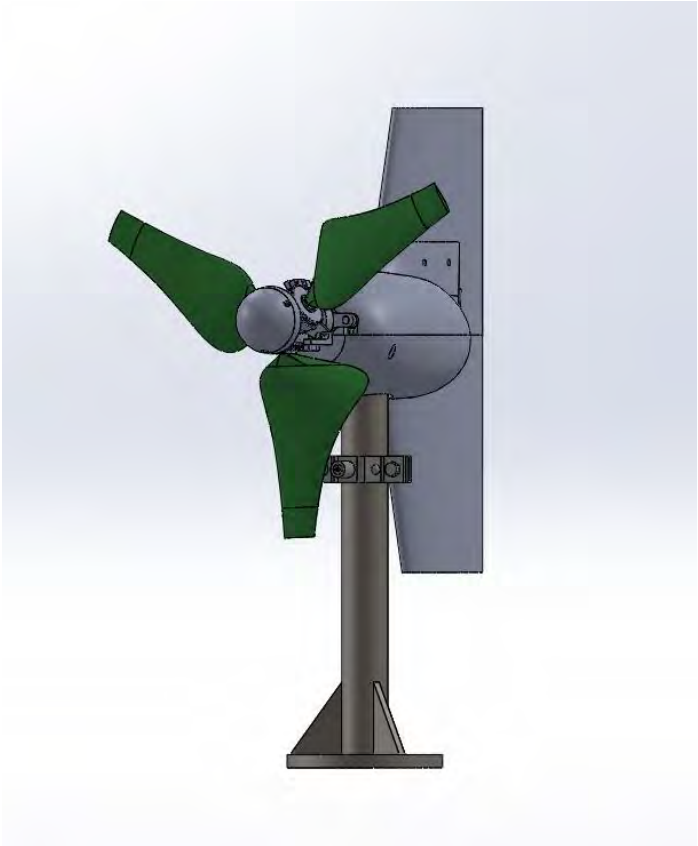

Table of Contents

Executive Summary

In this Report Cal Poly Wind Power Club details the conceptualization, analysis, prototyping, and testing of their small-scale wind turbine, affectionately named YAWS, for the Collegiate Wind Competition. The 2020-2021 competition was Cal Poly SLO's first time participating in the competition and this year the team is building upon the previous successes. It has been exciting transitioning to an in-person environment, giving the ability for greater collaboration, better sub-teams, and improved manufacturing abilities. The competition has been one of the club's major priorities for the academic year and has dictated the division of multiple teams and sub-teams. The major teams for turbine development consisted of an Aerodynamics team, Electrical team, Mechanical team. Within these divisions were more specialized groups of people including two senior projects, those being for the shallow water wind turbine foundation and the electronic team dynamic load. The main goal of this year was to base the designs of our turbine on what we had last year but identify and improve upon previous problems. Throughout the year we have made major strides to improve upon almost every element of our first iteration of the turbine.

Figure 1: The completed turbine, YAWS, on the dry land testing tower.

Design Objective

Our objective for this year's turbine was to utilize what we had from our team model last year and improve upon it to increase power output at the rated wind speed. We took time to redesign our blades, upgrade our generator for increased power output, and entirely change the electrical load for our turbine. In addition to these things, we had to adjust our mounting system for the turbine as we had to mount our turbine in water due to the constraints of this year's competition. We worked with an engineering senior design team who created the underwater foundation that we use with our turbine.

The upgraded components from our turbine from last year help us maximize our power output, reduce vibrations in our turbine, and improve our design overall. We selected a new set of airfoils for the blades and redesigned them for an ideal operating condition of 11 m/s. The underwater foundation allows us to mount our turbine in a way that mimics offshore windfarm conditions. The foundation has shear keys on the bottom to allow us to secure the foundation in the sand. This ensures that the loads on the turbine during testing do not cause the turbine to fall over.

Load Analysis

Blades

For designing the blades from a structural perspective, we computed forces on the turbine with a MATLAB script we wrote that computes the net force acting on the blade, and the equivalent moment concentrated at the root of the airfoil. This calculation is based on airfoil performance data collected through QBlade and extrapolated across 360 degrees using the Montgomerie method. The lift and drag forces are then calculated across each blade element, based on the chord length and angle at each particular section.

In the parked condition, the only forces present are those due to gravity, and the wind hitting the blades strongly pitched. For our turbine, the maximum pitching angle is 20 degrees, at a 22 m/s wind speed, this creates a drag force (which in this case acts horizontal, or parallel to the shaft of the turbine) of 1.72 N. The net lift force would be 3.17 N, across the plane of rotation.

When operational, at the max wind speed of 22 m/s at 2200 rpm, and a pitch angle of 0 degrees, the loads produced on the turbine are a force of 5.25 N along the shaft and 7.81N along the plane of rotation. These loads correspond with an equivalent moment at the dovetail of 0.60 Nm along the shaft and 0.97 in the direction of rotation.

To determine the strength of the part, specifically the dovetail as this is the weakest point, we performed static testing on the blade and determined that the critical direction is the force along the shaft, which could sustain a maximum moment of 1.29 Nm. This gives us a safety factor of 8.9 when parked and 2.15 when operational.

Center of Mass

With the change from a well-fixed mounting platform to the sand mounting platform we found a significant reduction in stability. As such, we had to take care in leveraging the design of the center of gravity to help us in preventing tipping when under a wind load, by centering the center of mass about the turbine tower. Another improvement to our center of mass this year was the removal of our laser tachometer which was mounted off to the side creating a left heavy imbalance. It was replaced with a hall effect sensor mounted at the back center of the generator mount. The sensor is smaller and lighter and will no longer contribute to asymmetry.

Gyroscopic Loading

One of the additions of this year's competition that required a design adaptation from our team was the involvement of a water foundation. Our design to accommodate this feature included a much longer tower which resulted in an amplification of the forces and moments present. One of the resultant design problems that arose from the new foundation design was the increased effect of the gyroscopic moment created from yawing the turbine while the blades were spinning at high speeds. Small rotations could cause the turbine to tip over due to the sand base. To combat this, we decided to lock the yaw whenever we are testing with the water mounting system with a small attachable brake mechanism. We understand that this is not a long-term solution, but the mechanism is designed to be implemented during turbine operation, to activate the brake on the yaw when we have determined the turbine to be sufficiently yawed into the wind.

Foundation

For our geotechnical analysis, we determined the effect of our loading conditions on the sand beneath our structure to minimize the weight of the structure needed to maintain stability. Using the Marine Geological Handbook as a reference, we discovered a set of comprehensive analyses required to design a foundation with a configuration of flat plate and stakes [1]. The handbook suggested that we calculate the bearing capacity of the sand beneath our foundation and compare this capacity to the bearing pressure induced by the loads on our foundation [1]. If the *capacity* of the sand exceeded the *pressure*, or demand, then the foundation would not tip.

The loading of our foundation is extreme for its small size. Large horizontal loads like this often require foundations with much larger areas proportionally. The large moment applied creates a large *eccentricity*, which is a metric of how large the applied moment is compared to the self-weight of the foundation. High eccentricity creates a small *effective area*, *A'*, which describes how much of the foundation's area, A = 625 cm^2) is touching the sand. To combat this large eccentricity, we decided we needed more weight, a lower center of gravity, embedded deeper in the sand than originally expected. As shown in **Table 3**, our final effective area *A'* = 174 cm^2.

The bearing capacity of the soil is dependent upon the engineering properties of the soil profile, the shape and size of the foundation, the depth of embedment, the load direction, and the inclination of the ground surface. We used equation 4.1 from the Marine Geological Handbook to calculate the bearing capacity of the sand beneath our foundation as recommended for a shallow foundation in cohesionless soil [1].

$$Q_u = A'\left(q_c + q_q + q + q_\gamma\right) + PH_s\left(\frac{s_{ua}}{S_t} + \gamma_b z_{avg}\tan\delta\right) \qquad \text{Eq. 4.1}$$

Table 1: Variables used to calculate bearing capacity

Variable	Definition	Value	Unit
A'	Effective area	0.0174	m^2
q	Cohesion bearing capacity stress	0	N/m^2
q_q	Overburden bearing capacity stress	71297	N/m^2
q_γ	Friction bearing capacity stress	14660	N/m^2
P	Foundation perimeter	0.96	m
H_s	Side soil contact height	0.15	m
s_{ua}	Undrained shear strength	0	N/m^2
S_t	Soil sensitivity	1.00	-
γ_b	Buoyant unit weight of soil	9425	N/m^3
z_{avg}	Average depth of stakes	0.020	m
delta	effective friction angle	0	deg
Q_u	Bearing Capacity	85957	N/m^2
FS	Factor of Safety	1.05	-

In addition to finding the capacity of the soil beneath our foundation, we compared the bearing capacity to the bearing pressure applied to the soil because of the loading conditions induced on our foundation as explained in our static analysis. A schematic of the loading scenario is shown in **Figure 2**.

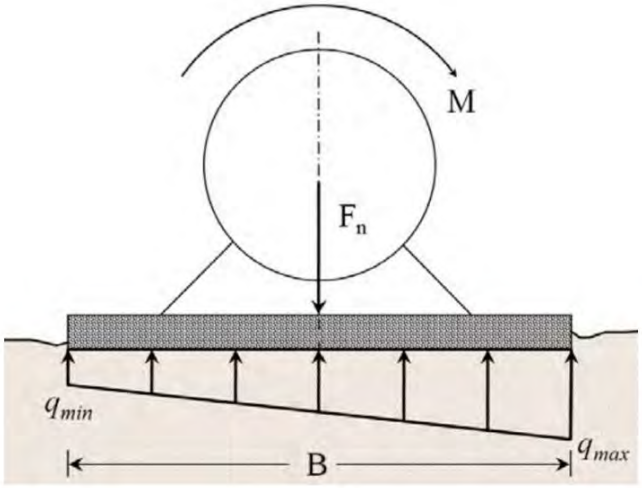

Figure 2: Bearing pressure distribution across a flat plate

Figure 2 demonstrates the bearing pressure distribution across a flat plate under an applied moment and normal force acting on the plate. To find this maximum bearing pressure induced on the soil from our loading conditions, we used the equation 4.2 from the handbook [1].

$$q_{max} = \frac{Fn}{BL} + \frac{6M}{(B^2)L} \qquad \text{Eq. 4.2}$$

Our base and length are set at 24 cm, which maximizes our foundation plate area while still allowing for a reasonable tolerance. The other variables used in equations 4.2 are defined in **Table 2** below.

Table 2: Variables used to calculate bearing pressure

Variable	Definition	Value	Unit
F_n	Normal bearing load	412.0	N
M	Applied moment	22.26	N-m
B	Foundation width	0.132	m
L	Foundation length	0.132	m
q_{max}	Bearing pressure	81864	N/m^2

Using a solver function in Excel, we set the foundation weight as our variable and defined our factor of safety to be 1.05. Our factor of safety has a narrow margin for error because it is important to reduce the weight of our foundation as much as possible and having minimal conservatism will help us reduce our final weight. Additionally, the consequences of failure are minimal because the wind speeds gradually approach the design speed, so any failure that occurs during testing will be easily identified and we will be able to safely reduce wind speed accordingly.

Lastly, to gauge the required foundation weight of our design needed at different wind speeds, we modified the wind speed in our solver function and computed the foundation weight required. **Table 3** contains these values of foundation weight at each wind speed using a factor of safety of 1.05.

Table 3: Calculated foundation weight at different wind speeds

Wind speed [m/s]	Foundation Weight [lbf]
7	31.11
8	42.00
9	56.65
10	75.13
11	97.87
12	125.55
13	159.24
22	1141.84

As you can see from **Table 3**, our current foundation design needs to weigh 75.13 lb. to withstand wind speeds of 10 m/s. This weight only includes the weight of the foundation and does not include the weight of the turbine. Given the analysis we performed based on our design, it would be impossible to make our foundation heavy enough to support the maximum wind speeds required by the competition. We aim to validate our design through simulated load testing as discussed in the testing section below.

Given the high weight required to avoid bearing failure of our foundation, we were able to construct the foundation with thick enough steel to avoid any failure of the structure itself. An FEA simulation of our loading resulted in a minimum safety factor of 16.

Electronics

To harvest maximum power, the brushless DC Odrive D5065 Dual Shaft Motor was selected to be used as a generator. The D5065 was chosen for its high, no-load speed which indicates that the turbine can generate power at low cut in speeds. Additionally, the ODrive motor was designed to be used with a motor encoder. The encoder enables the measurement of rotor speed as well as producing a feedback loop to control the speed.

At lower wind speeds, a higher load resistance produces more power. However, as the wind speed increases, the load resistance that maximizes the power output decreases. As a result, the dynamic load must change the resistance based on the wind speed. This is achieved with a circuit that uses a PWM signal from a microcontroller to vary the duty cycle based on the input voltage which is proportional to input wind speed.

A buck-boost converter was to be implemented to step down the voltage at high wind speeds and step up the voltage at low wind speeds to power the Arduino microcontroller. In last year's design, a 3-phase full bridge rectifier was included to convert the previous AC generator's output into DC power. Since we have selected a new generator that outputs DC voltage, the rectifier is no longer needed. However, a large capacitor is still included to reduce the ripple effect that is still present in the DC output of the generator.

Control Model

The pitch angle of the turbine blades is to be handled by a microcontroller. In this case, an Arduino Uno was chosen for its ease of use, for it being beginner-friendly, and most importantly its built-in Servo library that will be talked about in the software development section. The two modes of operation of this controller would allow for input to be taken either from the user, for cases like testing and experiments, or from the generator, for a full deployment case where the turbine is fully autonomous and would determine the best pitch angle based on voltage measurements of current generated power. The output of the controller is a pulse width modulation which acts as the encoded signal for the linear actuators to know what angle to adjust to. This then affects the angle of the blades and along with the incoming wind, the speed of rotation, and ultimately the power generated by the generator.

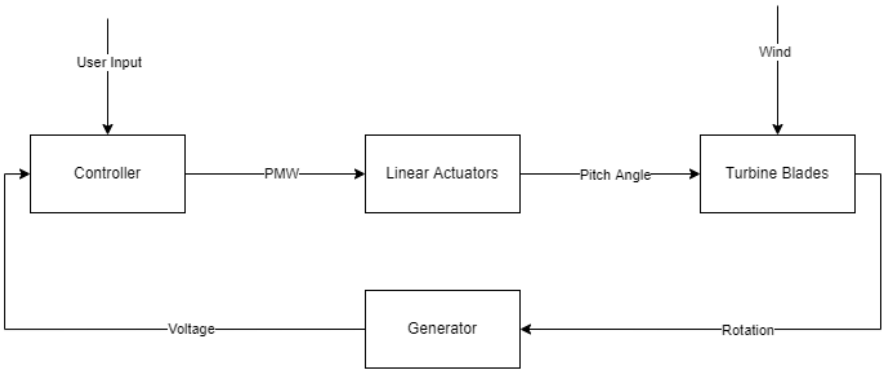

Figure 3: Tentative Control Flow for Pitching Mechanism

Software

The Pitching Angle Software was created in the Arduino IDE with files like the Arduino Servo Library. This is a handy library of useful predefined functions that allow for an easy setup of a Servo object that can control servos through different methods. The serial monitor was also used as an interface between the user and the Arduino during manual mode.

The first section of the code is the set up and initialization where the servo object and serial monitor are set up. Here the servo PWM signals for fully extended and fully retracted are defined. Additionally, the baud rate for the UART communication between the computer and Arduino is set. Lastly in the initialization, the position for the linear actuators is forced to start from the zero-angle position.

Next is input for changing the angle. This input can come from either the user, manual mode, or from reading a voltage from a pin on the board, auto mode. However, the software to enable automation of the pitch angle has not been complete. What is needed to finish it is data that describes the optimal pitch angle

for a given voltage and the associated mathematical equation describing such data. In either case, input is collected and tested if it is a valid input; if not it is ignored and waits for new input. This leads to the next phase which is testing if the new valid input is different enough from the previous angle to warrant a new change of angle. If the difference is big enough, this angle is then used as the angle with the servo object method to change the servo angle. This process repeats while there is still power connected.

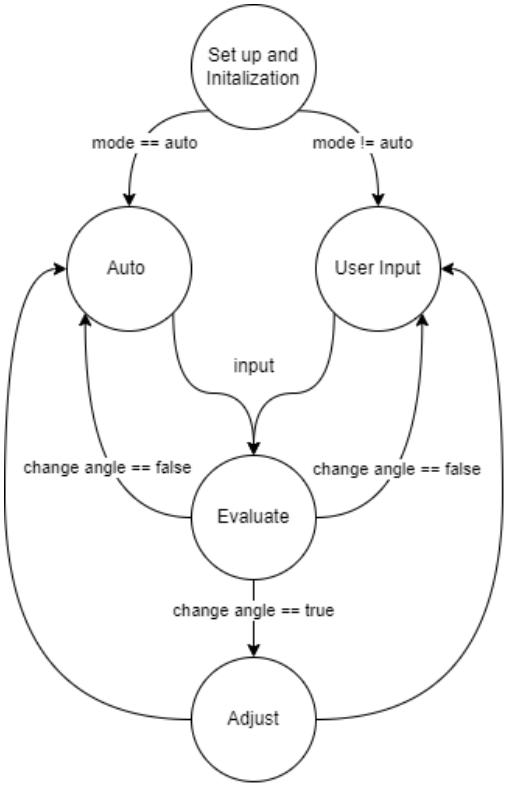

Figure 4: State Diagram for Pitching Angle Software

Final Assembly

Blades

The final blade design chosen was a modified combination of the S834, S833, and S835 airfoils with a 5.1 chord scale. This design was chosen after analysis using simulations and experimental data. After research of airfoils designed for low Reynolds numbers, four airfoil families were chosen for further examination. Using the open-source software, QBlade, the performance parameters for each blade were simulated and compared, paying special attention to the ratio of the coefficient of lift to the coefficient of drag. QBlade was also used to generate coefficient of lift and coefficient of drag data across ranges of angles of attack and extrapolate the data across 360 degrees of angles of attack using the Montgomerie method.

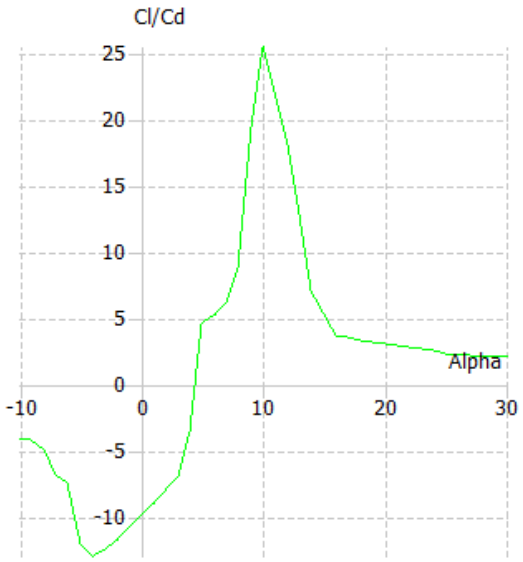

Figure 5: Coefficient of lift/drag vs angle of attack plot of the S833 airfoil. Thus, our turbine is designed to operate with the maximum efficiency at an angle of attack of 10 degrees.

We used this data in conjunction with our own MATLAB scripts based on Blade Element Momentum Theory to determine the optimal chord length and twist angle of each blade element. We also scaled the thickness of the chords by a value of 5.1, because we found through experimental testing that for these small blades, and possibly due to the variable nature of our fan-produced 'wind' for testing, the larger blade area resulted in greater power output. The lift and drag coefficient data was also used in the MATLAB script to determine predictions of lift and drag forces that were used to perform static testing of the blades to ensure structural soundness and operational safety.

The blades are manufactured using 3D printing, so the material properties are not necessarily consistent nor well documented. This was overcome by a statistical experiment used to analyze the effect of several 3D print factors on the strength of 3D printed blades, including the infill percentage, the airfoil span, and annealing. Using the experimentally determined print qualities for the highest strength, each blade was printed and statically loaded with the expected load and higher loads to confirm a factor of safety.

Once the blades passed the static loading test, they were tested in front of a fan at multiple wind speeds and the rotational speed was evaluated. The constant conditions and wind speeds allowed for the comparison of the performance of each blade design and led to the selection of a final airfoil class, the S833, S834, and S835 to proceed design with.

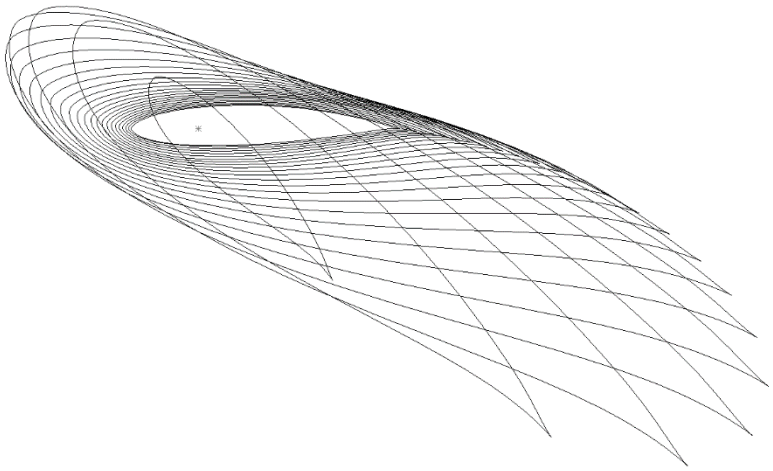

Figure 6: Sketches of each blade airfoil, looking at the blade along the z-axis. This view serves to highlight and emphasize the twist that takes place along the length of the blade at each cross section and the gradual transition between the airfoil shapes.

For the final design, the root airfoil, S835, is pure at 8% of the blade length. The main airfoil, S833, is pure at 75% of the length and the tip airfoil, S834, is pure at 96% of the blade length. To cover the span between these airfoils without causing discontinuities that would negatively affect the aerodynamic performance of the blade, we linearly interpolated between the coordinates of the airfoils to create intermediate airfoil profiles. These shapes can be seen in **Figure 6** above, as they appear along the blade, looking down the perspective of the z-axis.

The blades were manufactured via 3D printing to attain the complex geometry present in their structure as well as to be easily producible for repeated testing and comparison. They were designed to be compatible with the existing pitching mechanism via a dovetail tab and slot. The pitching mechanism uses a rack and pinion system initiated by linear actuators in the nacelle to adjust the blades' angle of attack based on the wind conditions for optimized performance as determined from our predicted ideal angles of attack. The pitching mechanism's linear actuators operate under the controls outlined previously. The pitching control is performed by the sub team managing the electronics but directed by the blade design team, which requires communication of target angles of attack when considering wind speed and rotational speed.

Figure 7: The final blade design situated into the pinions of the pitching mechanism. This unit is mounted onto the shaft and a nose cone is placed upwind for best airflow.

Rotor

The aerodynamic lift generated by the wind speed at the blades drives the rotor, driveshaft, and consequently the generator from the front of the turbine. Also located on the front of the turbine is the pitching mechanism. These components are secured onto the shaft with a lock washer and nut which are then covered by a nose cone for improved aerodynamic performance. The pitching mechanism has the same design as last year.

Drivetrain

The shaft design was kept the same as our previous turbine and has a safety factor greater than six. The dimensions of the steel shaft could have been made smaller; however, they were kept at the current dimensions for the consideration of necessary bearings and ease of manufacturing. The bearings supporting the shaft are 10- and 12-mm diameter ball bearings, and smaller bearings are challenging to find and purchase. The couplings also use the same system, but we had to change the diameter to accommodate the new generator which has a different shaft size.

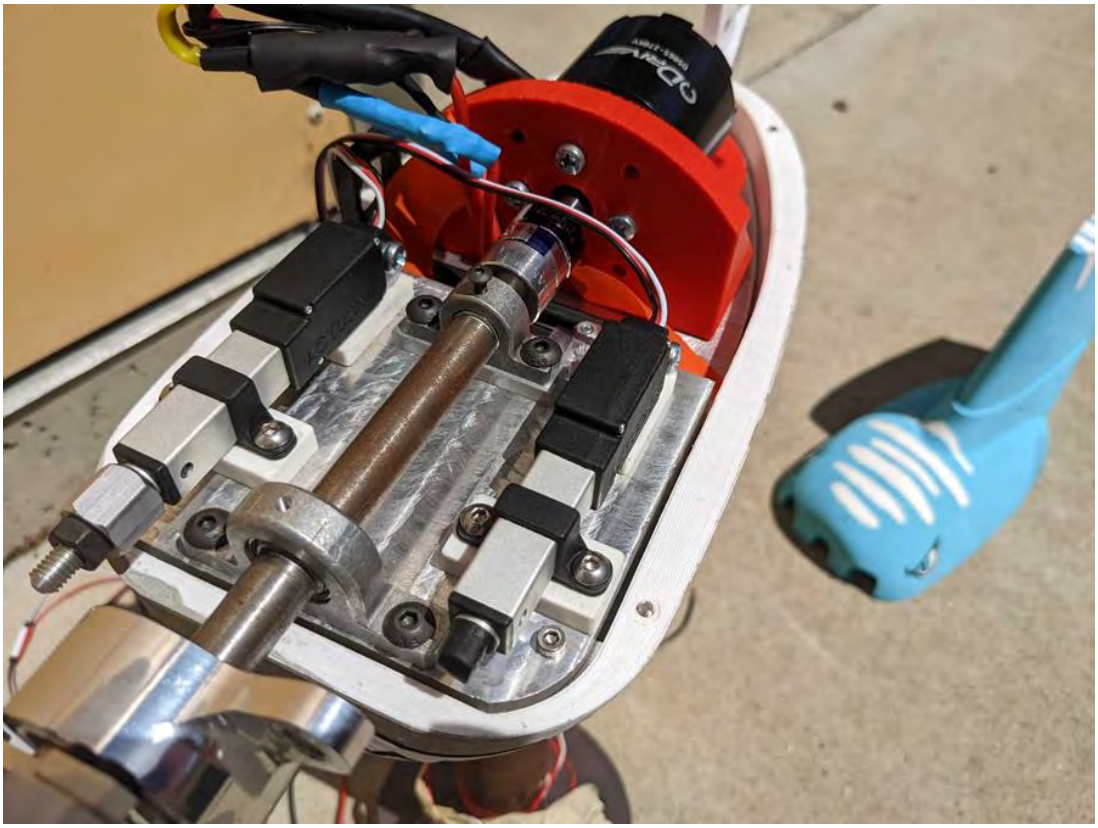

Figure 8: The drivetrain assembly and linear actuators for the pitching mechanism, most of which were maintained between years.

Nacelle

The nacelle houses the shaft and its supporting components as well as the generator and other electronics. The largest concern when designing the base plate dealt with layout, the center of gravity, and ease of assembly/maintenance. The base plate of the nacelle supports the bearings that align the shaft with the generator for minimal vibrations and low mechanical load supported by the generator. Additionally, there is a cut out in the baseplate in which we can install various generator mounts for a wide range of generators that were useful early in development while we were still testing different generators. The linear actuators that drive our pitching mechanism are also installed on the base plate. Many of the mounts within nacelle are 3D printed to allow for rapid and lower cost alterations that give us more flexibility while iterating. The nacelle also incorporates a tail fin that will cause the turbine to passively yaw into the wind when desired.

Foundation and Tower

The foundation subsystem consists of an above-ground system, below-ground system, and tools and installation system. The above-ground system utilizes welded support members connecting the foundation tower to the foundation plate which is the common connection between the two systems. The below-ground system is attached via M10 bolts that feed through the foundation plates and are secured with nuts above the top plate. The number of foundation plates used is dependent on the desired wind speed at which to test the turbine. The below-ground foundation plate is where the shear keys are attached. Each shear key (labeled stakes in **Figure 9** below) is attached with M6 screws that thread into tapped holes in the plate.

The steps outlined above are to be completed before the installation time begins during a testing event. The foundation is assembled entirely before installation. During installation time, installers will first use shovels to push sand away from the center of the tank, where the foundation is to be installed. Next, an installer

will use a tamper to compact the sand in the center, where the foundation will be placed. Once the sand is packed, the team will lower the foundation into the tank by hand, being sure not to touch the water, and push it into the sand, then will use the water above the foundation to rinse off the tamper, allowing sand to settle on top of the foundation. When the foundation is in place, the installers will place a piece of soft, buffer material on top of the foundation tower, and use the tamper to pound the foundation deeper into the sand, until the top of the tower is at an acceptable distance from the top of the tank.

Once the foundation is secured in place, the team will check level with the bubble level, and level the foundation as needed by using a wooden member and a dead blow to apply directed strikes to the edges of the foundation until the foundation is level. The distance between the foundation tower and the top of the tank is once again checked, and the stub and turbine are attached.

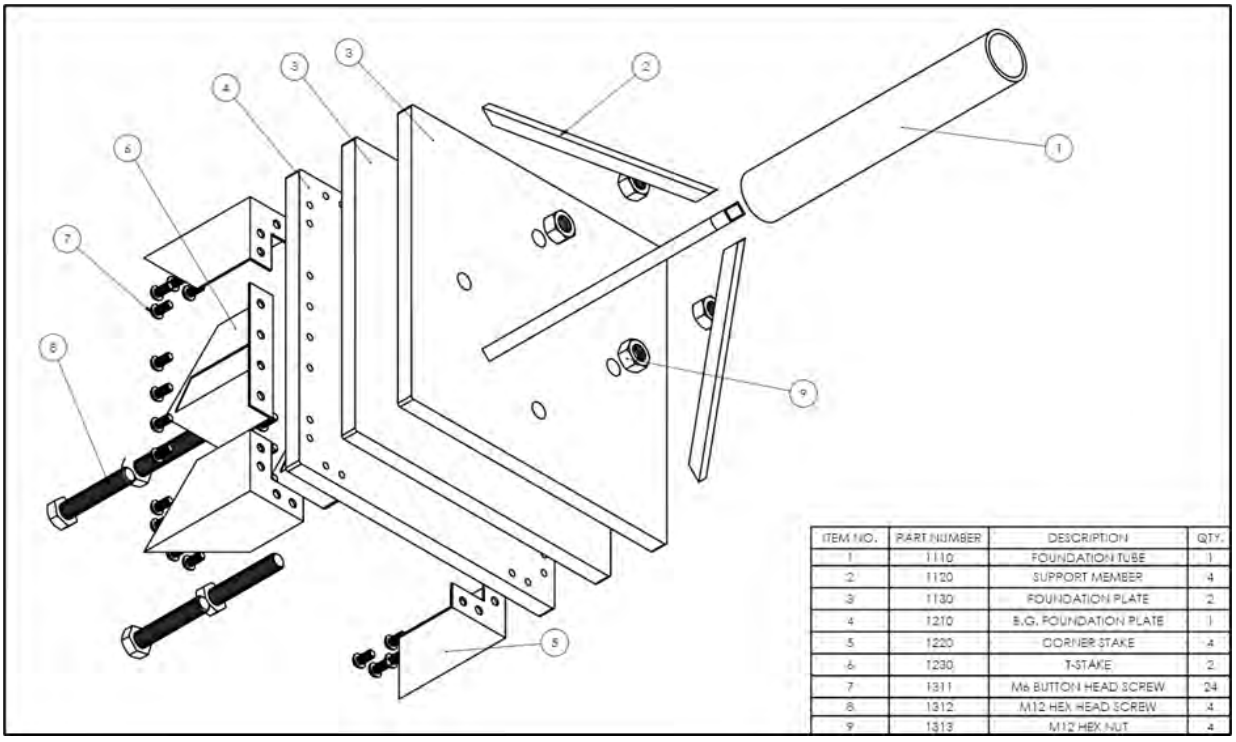

ITEM NO.	PART NUMBER	DESCRIPTION	QTY.
1	1110	FOUNDATION TUBE	1
2	1120	SUPPORT MEMBER	4
3	1130	FOUNDATION PLATE	2
4	1210	E.G. FOUNDATION PLATE	1
5	1220	CORNER STAKE	4
6	1230	T-STAKE	2
7	1311	M6 BUTTON HEAD SCREW	24
8	1312	M12 HEX HEAD SCREW	4
9	1313	M12 HEX NUT	4

Figure 9: Exploded view of foundation assembly

Turbine Electronics

A new generator was purchased to increase efficiency as well as eliminate the need for a 3-phase full bridge rectifier. The new DC Odrive motor can generate power at low revolutions per minute. The generator's output would be connected to a filtering capacitor to reduce ripple effects and create a steadier output. The capacitor would then connect to a voltage and current sensor that provides information to the pitching microcontroller that would be used to determine whether the blades need to be slowed down or sped up. The buck-boost converter would take the power from the generator to power the pitching microcontroller as well as the dynamic load microcontroller.

Load Electronics

The load electronics were similar to last year's design but featured some minor changes in resistance values according to the power curve for this year's turbine. The resistance of the dynamic load is varied between 23-60Ω with larger resistances at lower wind speeds and smaller resistances at lower wind speeds. The load utilizes a microcontroller to create a pulse-width modulated signal based on the sensed input voltage which is proportional to the input wind speed. This PWM signal then is fed to a gate driver which quickly switches

the gates of two power NMOS on and off according to the PWM. When both gates of the NMOS are on, current flows through all three branches of the dynamic load, causing the resistance seen at the load to be 23Ω as all three resistances are placed in parallel. When both NMOS gates are turned off, no current flows through those two branches and so the resistance seen at the load is 60Ω as that is the resistance connected when current only flows through one branch.

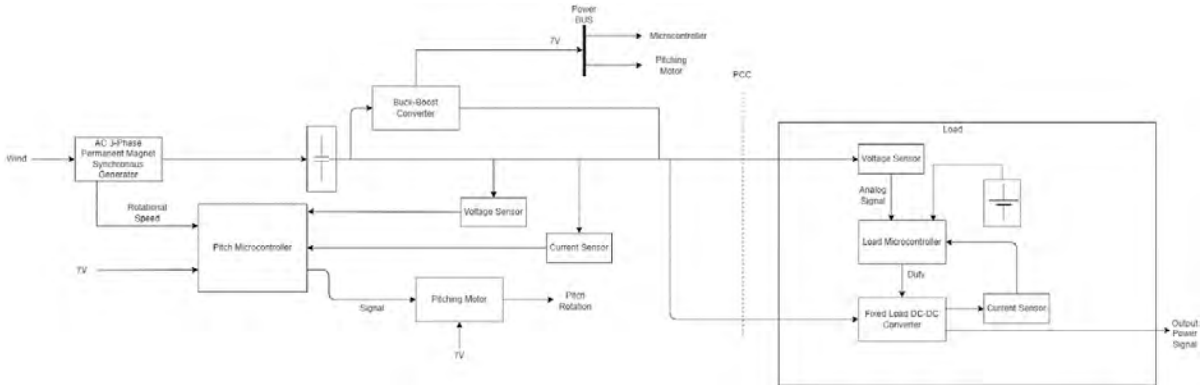

Figure 10: Turbine Electronics and Load Electronics Black Box diagram

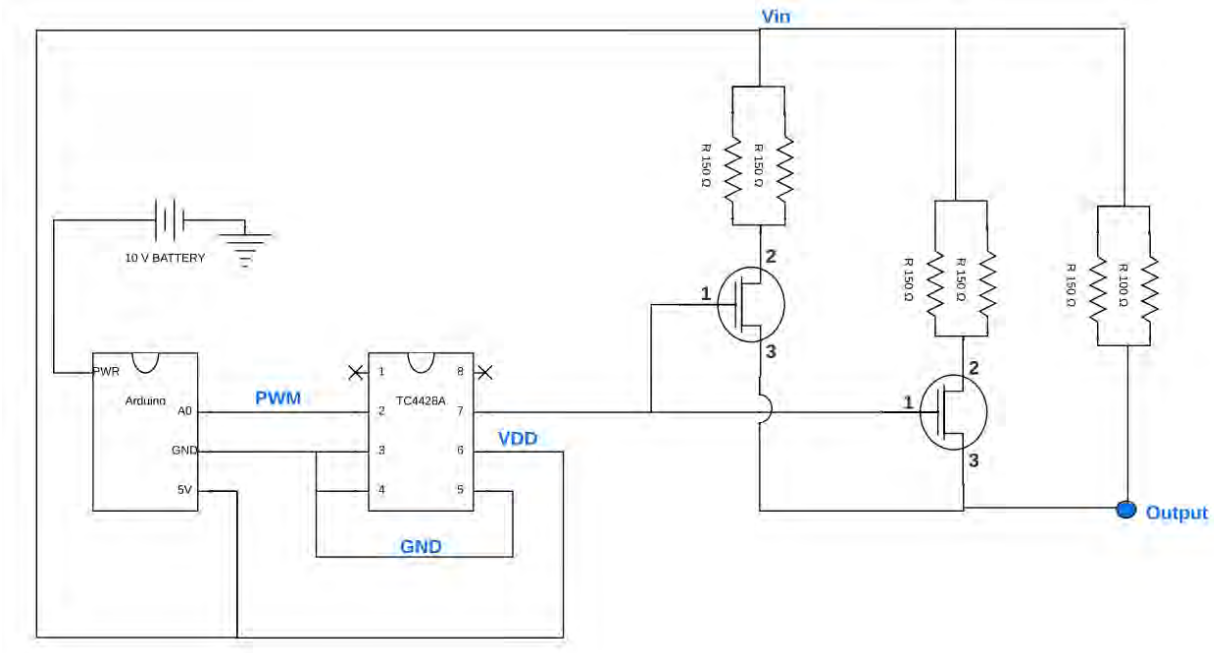

Figure 11: Component Diagram of Dynamic Load

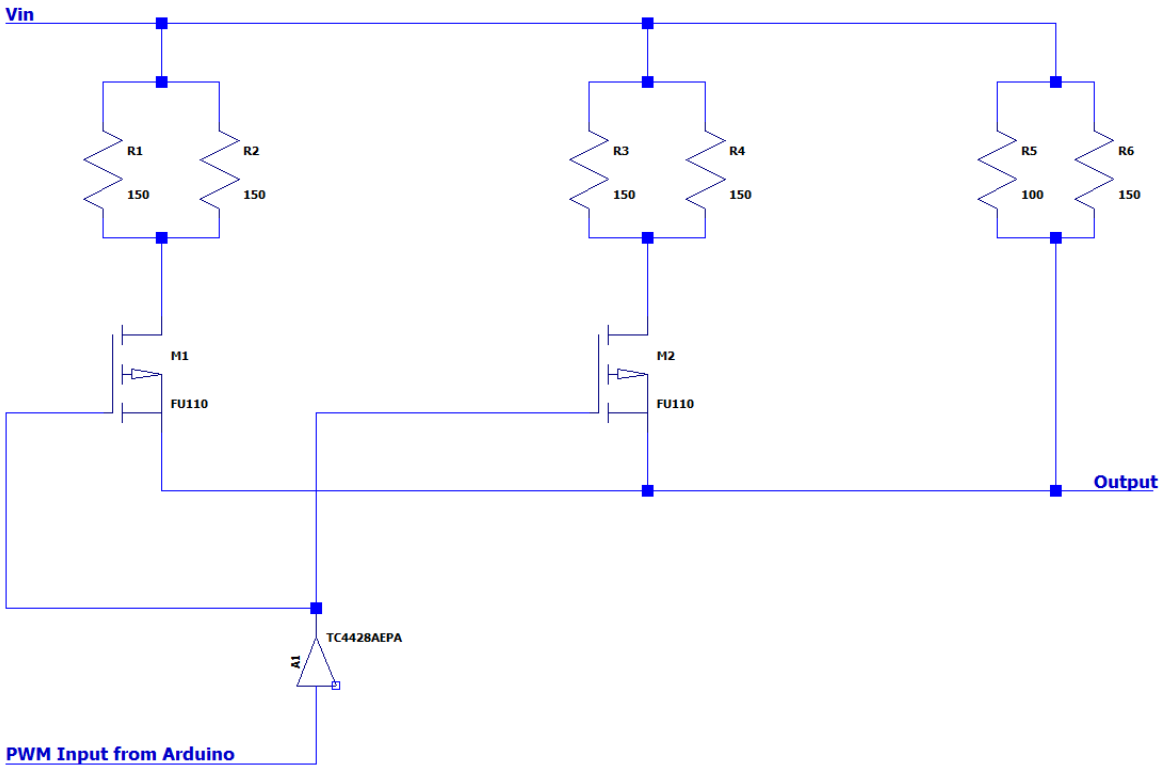

Figure 12: Schematic of Dynamic Load

Assembly and Commissioning Checklist

Step	Completed
Lower bottom portion of nacelle cover around tower	
Insert slew bearing assembly into top of tower and bolt in place	
Bolt base plate onto slew bearing assembly Do not overtighten as it increases slew friction	
Raise bottom portion of nacelle cover and bolt to bottom of base plate	
Attach onboard components to baseplate • Bearing mount • Pitching actuator and mount • Generator mount	
Bolt generator onto mount	
• Insert hall effect sensor onto back of generator mount	
Feed control wires down tower	
Insert shaft and bearings into bearing mount Use set screws to fasten bearings and couplings	
Load blades into pitching mechanism dovetail	
• Place pitching mechanism onto end of shaft	
Align and attach actuators to pitching mechanism	
Place top half of nacelle onto base plate and bolt in place	
Attach nose cone and nut to tip of shaft	
Install foundation	
Attach tower to the foundation	

Testing

All our testing has been conducted in a field setting. Our primary concern while testing the blades was aerodynamic performance and failure at the base of the blade where it is held by the dovetail. Previous experience and testing suggested that this was the most common failure point. Our initial testing began with 20 combinations of airfoils and dovetail designs. Each blade was clamped in a testing fixture and loaded with increasing weight at a fixed point from the dovetail until failure. Custom MATLAB code was written to calculate theoretical blade loads at a wide range of pitch angles, wind speeds, and designs. This code was used to determine which of our combinations met minimum strength requirements. Further testing was done to compare the material properties produced by different 3D printing parameters such as layer height, extrusion rates, and heat treating. Once we had settled on printing parameters, we conducted another round

of static tests on a narrowed pool of blades using the same testing configuration before moving on to spinning tests. After dynamic testing across a range of wind speeds using a fixed-pitch hub, we determined that the S833 produced significantly higher RPM at the same load as our other blades. We used our custom MATLAB code along with Qblade data to determine the theoretical optimal pitch angle.

The foundation was first tested for structural integrity, which was not an issue, as predicted. The foundation was then installed into the sand, using the procedure described above up until attaching the stub, and timed. Through seven trials, successful installation times have ranged from five and a half minutes to eight and a half minutes, leaving a significant amount of time to attach the stub and turbine. The foundation then underwent simulated load testing to ensure it would not fail under turbine operation conditions. Through two trials with two plates attached to the welded structure, the foundation is performing better than our calculations predicted, but more testing is needed to verify our analysis. As of the time of writing, the entire turbine assembly has not been tested due to delays in manufacturing and unforeseen issues with the linear actuators in the pitching system.

Engineering Diagrams

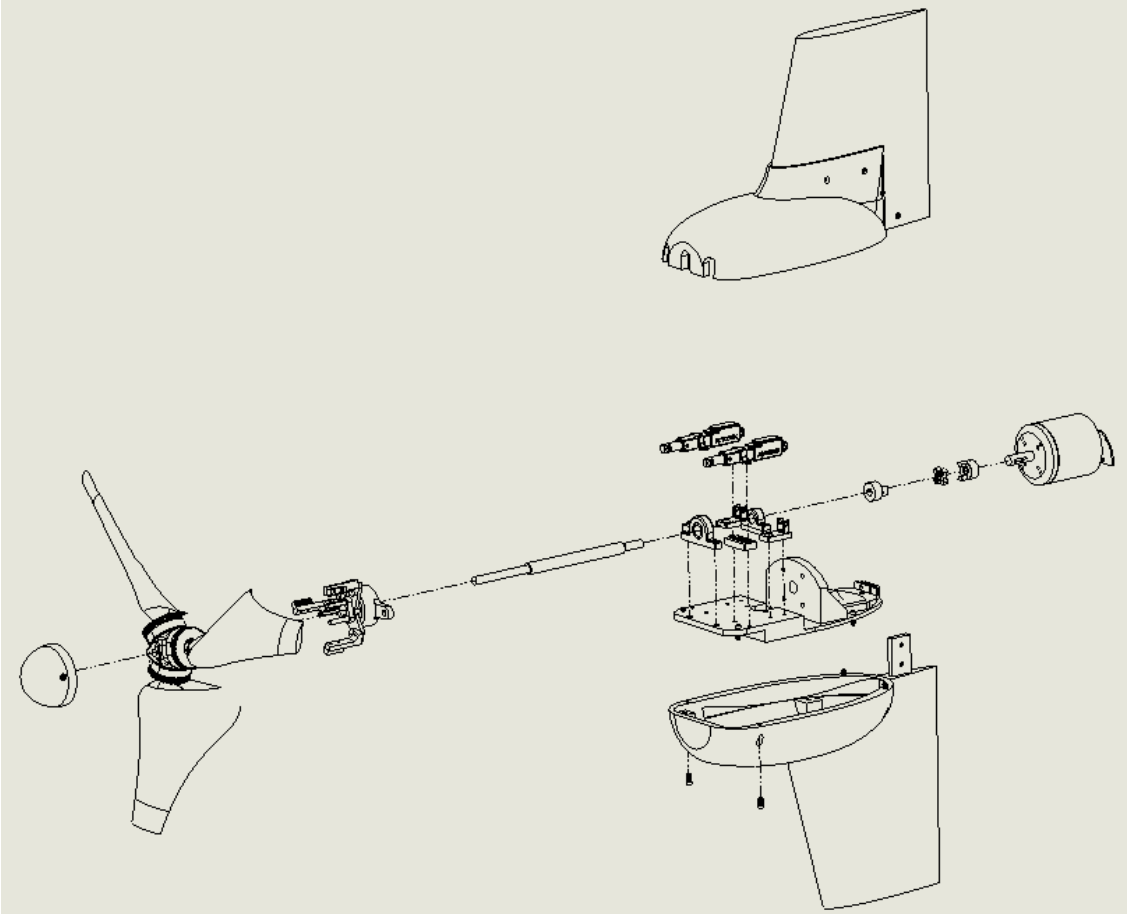

Figure 13: A brief depiction of the general assembly of the components in the nacelle

Maintained Designs

This being the second year working with the competition we had identified many weak points in last year's turbine which we focused on for iteration and improvement this year. Other components we found to be in a state where they could remain the same.

Nacelle Housing and Tower

Firstly, the nacelle housing and above-water tower have remained largely the same. The only modification made to the tower was an added component to lock the yaw in place to reduce the gyroscopic moment when the turbine was active. Overall, though, the components of our nacelle still fit into the existing housing, so for the sake of reduce manufacturing time and to reduce the amount of plastic used, the nacelle cover was left untouched aside from a paint job. Even with all the changes that were made, the net weight of the nacelle did not change much so the tower and attached slew bearing were kept.

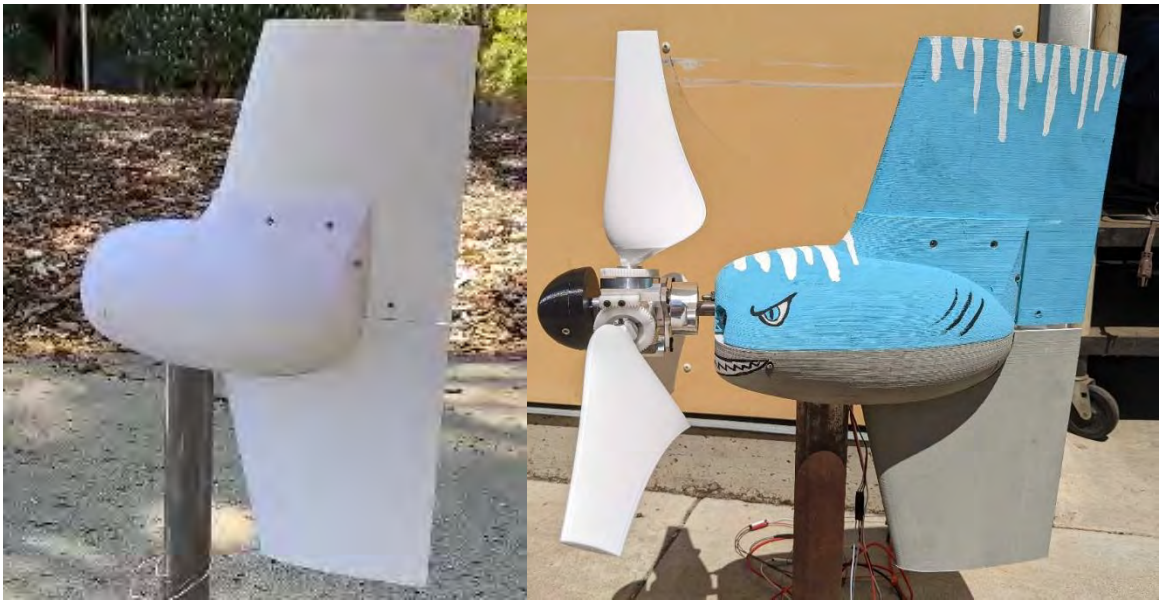

Figure 14: The 2021 and 2022 nacelle covers

Pitching Mechanism

Additionally, we utilized the same mechanical pitching mechanism as last year, however, major changes were made to the code behind it. The existing pitching mechanism was the result of a team-sponsored senior design project and was the product of nine months of design work and effort by the senior project group. Given all the thought and engineering practice that determined this as the best solution to perform our pitching, we chose to do minimal tampering. The physical mechanism was functional last year but the code driving it was imperfect and difficult to use which hindered us from getting the most out of a crucial and well-engineered component of our turbine. This year it is fully operational and from testing, we have noticed a significant increase in the performance of the pitching subsystem from the code improvements.

Drivetrain

The drivetrain also received no major updates outside of minor changes to the shaft and couplings to mate with the new generator. Last year's shaft was designed to withstand loads and speeds even greater than those achieved with our new blade geometry, as such we did not feel it necessary to make major changes. Aside from these components, all other subsystems received major design updates based on the lessons we learned last year.

References

[1] Beasley, Diane Jarrah and David Thompson, *Handbook for Marine Geotechnical Engineering*, Port Hueneme, CA USA.